IJC Heart & Vasculature 8 (2015) 19–31

Contents lists available at ScienceDirect

IJC Heart & Vasculature

journal homepage: http://www.journals.elsevier.com/ijc-heart-and-vasculature

Distinct electrophysiological and mechanical beating phenotypes of long QT syndrome type 1-specific cardiomyocytes carrying different mutations

Anna L. Kiviaho [a,*,1], Antti Ahola [b,1], Kim Larsson [a,1], Kirsi Penttinen [a,1], Heikki Swan [c,1], Mari Pekkanen-Mattila [a,1], Henna Venäläinen [a,1], Kiti Paavola [a,1], Jari Hyttinen [b,1], Katriina Aalto-Setälä [a,d,1]

[a] University of Tampere, BioMediTech, School of Medicine, Tampere, Finland
[b] Tampere University of Technology, Department of Electronics and Communications Engineering, BioMediTech, Tampere, Finland
[c] Heart and Lung Center, Helsinki University Central Hospital, University of Helsinki, Helsinki, Finland
[d] Heart Center, Tampere University Hospital, Tampere, Finland

ARTICLE INFO

Article history:
Received 8 April 2015
Accepted 16 April 2015
Available online 25 April 2015

Keywords:
Long QT syndrome
Induced pluripotent stem cell
Arrhythmia
Patch clamp
Calcium imaging
Digital image correlation

ABSTRACT

Background: Long QT syndrome (LQTS) is associated with increased risk of ventricular arrhythmias and cardiac arrest. LQTS type 1 (LQT1), the most prevalent subtype of LQTS, is caused by defects of slow delayed rectifier potassium current (I_{Ks}) that lead to abnormal cardiac repolarization. Here we used pluripotent stem cell (iPSC)-technology to investigate both the electrophysiological and also for the first time the mechanical beating behavior of genetically defined, LQT1 specific cardiomyocytes (CMs) carrying different mutations.
Methods: We established *in vitro* models for LQT1 caused by two mutations (G589D or ivs7-2A>G). LQT1 specific CMs were derived from patient specific iPSCs and characterized for their electrophysiology using a current clamp and Ca^{2+}-imaging. Their mechanical beating characteristics were analyzed with video-image analysis method.
Results and conclusions: Both LQT1-CM-types showed prolonged repolarization, but only those with G589D presented early after-depolarizations at baseline. Increased amounts of abnormal Ca^{2+} transients were detected in both types of LQT1-CMs. Surprisingly, also the mechanical beating behavior demonstrated clear abnormalities and additionally the abnormalities were different with the two mutations: prolonged contraction was seen in G589D-CMs while impaired relaxation was observed in ivs7-2A>G-CMs.
The CMs carrying two different LQT1 specific mutations (G589D or ivs7-2A>G) presented clear differences in their electrical properties as well as in their mechanical beating behavior. Results from different methods correlated well with each other suggesting that simply mechanical beating behavior of CMs could be used for screening of diseased CMs and possibly for diagnostic purposes in the future.

1. Introduction

Long QT syndrome (LQTS) is an electric disorder of the heart that predisposes patients to arrhythmias and sudden cardiac death. The arrhythmias related to LQTS are distinctive ventricular arrhythmias called Torsades de Pointes (TdP) [1]. LQTS type 1 (LQT1) is the most prevalent subtype of the disease. It is caused by mutations in *KCNQ1* gene encoding the α-subunit of the channel responsible for the slow component of the delayed rectifier potassium current (I_{Ks}) [2,3]. The inadequate I_{Ks} current leads to prolongation of repolarization time of action potentials (APs) in single CMs and to prolonged QT interval seen in electrocardiogram (ECG). Various mutations in *KCNQ1* have been identified to cause LQT1 possibly with varying clinical phenotypes [4,5].

Currently different LQTS subtypes are diagnosed with gene mutations in particular genes. However, there is a huge spectrum of mutations in each gene and the severity of the disease has been observed to be more dramatic due to mutations in some genetic regions compared to others [4,6]. Also in cell culture studies with transfected cells, different mutations in the same gene have had different effects on the electrical properties of the cells [7,8]. While some mutations (*e.g.* G589D) seem to have rather mild and recessive effect on the I_{Ks} current [8], other mutations (*e.g.* ivs7-2A>G) cause a complete loss-of-function of the I_{Ks} channel in a dominant negative fashion [7]. Little is known about the mechanisms of the ivs7-2A>G to cause the loss-of-function effect on I_{Ks} current while G589D mutation seems to be a clear trafficking mutation with normal functioning of the channel but with hindered transportation to the plasma membrane [9].

With induced pluripotent stem cell (iPSC) technology, it is possible to generate genetically defined stem cell lines [10,11] and differentiate

* Corresponding author at: Biokatu 12, FI-33014, University of Tampere, Finland. Tel.: +358 40 190 1765; fax: +358 3 3641501.
E-mail address: anna.kiviaho@uta.fi (A.L. Kiviaho).
[1] This author takes responsibility for all aspects of the reliability and freedom from bias of the data presented and their discussed interpretation.

http://dx.doi.org/10.1016/j.ijcha.2015.04.008

these into any cell type of interest. Thereby, *e.g.* LQTS-specific CMs can be generated and studied *in vitro* [12–18]. Traditionally the functionality of CMs in cell culture is determined by electrical or optical analysis, such as patch clamp-technique and microelectrode array (MEA) or calcium (Ca^{2+})-imaging and voltage sensitive probes. However, all these methods have some limitations. Patch clamp-technique is time consuming as well as invasive and cells die after measurements. Voltage sensitive dyes and the tracers used in Ca^{2+}-imaging may alter the electrophysiological properties of CMs and the cells may also be damaged by photo-toxicity [19] or compartmentalization [20] and cells die after analysis. MEA can efficiently be used for cell clusters but due to the physical dimensions of the electrodes and limitations in the sensitivity, it is not suitable with single cells. In addition, these methods detect only ion fluxes that obviously are important but some other, currently even unknown factors influencing the beating of CMs may be neglected. The analysis of mechanical beating properties could reveal additional information beyond the electrical phenomena and this analysis is neither invasive nor toxic and cells can be monitored for a long time.

In this study we present the electromechanical properties of LQT1-CMs having different mutations in the *KCNQ1* gene (G589D or ivs7-2A>G). The electrical and mechanical behavior of the cells was analyzed using a single cell current clamp, Ca^{2+}-imaging and light microscopy video-image analysis. CMs with either of the LQT1-genotypes had significantly prolonged APs, but only CMs with G589D mutation had spontaneous early afterdepolarizations (EADs) at baseline. Additionally, also abnormal Ca^{2+} transients were observed in LQT1-CMs. We also demonstrate that the mechanical beating behavior of the CMs with different *KCNQ1* genotypes has distinct mutation-specific features. This is the first published work where mechanical beating properties of LQTS are studied at the single cell level and the first evidence that LQTS can be detected by monitoring the mechanical beating of the cells.

2. Methods

The study was approved by the ethical committee of Pirkanmaa Hospital District (R08070) and written consent was obtained from all fibroblast donors.

2.1. Clinical information

LQT1 patient carrying G589D mutation is a 46-year-old female with corrected QT interval (QTc) of 464 ms. She has been suffering from syncopal spells. The other LQT1 patient is a 51-year-old female carrying ivs7-2A>G in *KCNQ1*. She has suffered from dizziness, darkening of vision and episodes of unconsciousness. Her QTc is 489 ms. Both of these patient are on β-blocker medication. Control iPSCs were generated from a healthy female, 55 years of age with QTc of 406 ms. The patients with LQT1 were on beta blockers and no irregularities in the QTc were found in the resting condition (Fig. 3 A–C).

2.2. Cell culture conditions

Primary fibroblasts from the skin biopsy were cultured under fibroblast culturing conditions using Dulbecco's modified Eagle medium (DMEM, Lonza, Basel, Switzerland) with 10% FBS (Lonza), 2 mM glutamax (Life Technologies Ltd, Paisley, UK) and 50 U/ml penicillin/streptomycin (Lonza). 293FT-cells (Life Technologies Ltd) were cultured in the same conditions with 1% nonessential amino acids (NEAA, Cambrex, East Rutherford, NJ, USA). Plat-E-cells (Cell Biolabs, San Diego, CA, USA) and irradiated/mitomycin C (Sigma-Aldrich, St. Louis, MO, USA) treated mouse embryonic fibroblasts (MEF) (Millipore, Billerica, MA, USA) were maintained similarly but without antibiotics. iPSCs were sustained together with MEF feeder cells in KSR-medium containing knockout (KO)-DMEM (Life Technologies Ltd), 20% KO-serum replacement (KO-SR, Life Technologies Ltd), NEAA, glutamax, penicillin/streptomycin, 0.1 mM β-mercaptoethanol (Life Technologies Ltd), and 4 ng/ml basic fibroblast growth factor (bFGF, R&D Systems Inc., Minneapolis, MN, USA). All the cells were grown at 37 °C and 5% CO_2 and the medium was changed every other day for iPSCs and two times a week for all the other cells.

2.3. Generation and characterization of iPSC lines

The LQT1 patients carried either the G589D mutation of *KCNQ1* (*KCNQ1*-FinA) or the ivs7-2A>G mutation in *KCNQ1* (*KCNQ1*-FinB) [21]. Skin biopsies from the donors were cultured in 0.2% gelatin (Sigma-Aldrich)-coated flasks under fibroblast culturing conditions. iPSC lines were established using lentivirus infection followed by retrovirus infection. The full protocol has been described by Takahashi and colleagues[10]. Cells, plasmids and reagents used in this protocol include: 293FT cells, Plat-E cells, pLenti6/UbC/mSlc7a1-vector (Addgene, Cambridge, MA, USA), ViraPower™ Packaging Mix (Life Technologies Ltd), Lipofectamine™ 2000 (Life Technologies Ltd), Fugene 6 (Roche Diagnostics, Mannheim, Germany), and pMX retroviral vectors (hOCT3/4, hSOX2, hKLF4 and hc-MYC, all from Addgene). Several lines were established from both patients and from control individual and two from each were selected for further characterization. Studied cell lines were UTA.00208.LQT1 and UTA.00211.LQT1 generated from *KCNQ1* patient with G589D mutation, UTA.00102.LQT1 and UTA.00118.LQT1 generated from *KCNQ1* patient with ivs7-2A>G mutation, and UTA.04602.WT and UTA.04607.WT generated from healthy control individuals.

Characterization of control iPSC lines is described in detail by Ahola and colleagues [22]. LQT1 specific iPSCs were characterized similarly by RT-PCR, immunocytochemistry, embryoid body (EB) and teratoma formation. Teratomas were generated from one control iPSC line (UTA.04602.WT) and two LQT1-lines one carrying G589D mutation and the other ivs7-2A>G in *KCNQ1*. In addition, the karyotypes of all the lines were analyzed. The lines were also assayed with PCR and restriction reactions to detect the correct mutations of *KCNQ1* from the genomic DNA and the control iPSC line was verified not to carry these mutations. DNA was isolated using DNA Tissue XS-kit (Macherey-Nagel GmbH & Co., Düren, Germany) and multiplied with AmpliTaq 360 Polymerase (Life Technologies Ltd) with 100 ng of template, 2 mM of $MgCl_2$, 200 μM of NTPs, 0.5 μM of primers (G589D forward: ttg act ctc agc tac ctc cc, reverse: tgc agg agc ttc acg ttc ac, ivs7-2A>G forward: ggg gag ctg tag ctt cca ta, reverse: agc caa atg cat ggt gag at, Biomers.net GmbH, Ulm, Germany), and 1 U/ μl of enzyme in total volume of 40 μl. Reaction conditions: 96 °C for 10 min (96 °C for 30 s, 60 °C for 30 s, 72 °C for 2 min), 35 cycles, 72 °C for 5 min. Digestion for *KCNQ1*-G589D was done with HIN6I (Thermo Fisher Scientific, Inc., Waltham, MA, USA) with Tango Buffer (Thermo Fisher Scientific, Inc.), and for *KCNQ1*-ivs7-2A>G with Dde1 (Thermo Fisher Scientific, Inc.) using FastDigest Buffer (Thermo Fisher Scientific, Inc.) both with 10 μl from PCR in total volume of 20 μl at 37 °C over night. Products were run on 4% agarose gel (EuroClone S.p.A., Milano, Italy): wild type (WT) for G589D (G589D-WT) generates product sizes 146, 82 and 39 bp, heterozygote (Hez) for G589D (G589D-Hez) generates an extra fragment of 185 bp, ivs7-2A>G-WT produces sizes 228, 39 and 33 bp and ivs7-2A>G-Hez an extra product with size of 261 bp. Extra fragments are caused by vanishing of the cleavage sites due to the mutations (G589D: 146 + 39 = 185, ivs7-2A>G: 228 + 33 = 261) (Fig. 2).

2.4. Cardiac differentiation and immunocytochemical characterization of CMs

CM differentiation was accomplished by co-culturing iPSCs with END-2 cells (a gift from Prof. Mummery, Humbrecht Institute, Utrecht, The Netherlands). END-2 cells were cultured as described by Mummery and colleagues [23]. Differentiation was initiated by dissecting the undifferentiated iPSC colonies mechanically into aggregates containing a few hundred cells. These cells were then plated onto mitomycin

C-treated END-2 cells in KSR medium without serum, serum replacement, or basic fibroblast growth factor but with 2.92 mg/ml of ascorbic acid [4] (Sigma-Aldrich). The cell colonies were monitored daily by microscopy, and the medium was changed after 5, 8, and 12 days. After 14 days of culturing, 10% serum replacement was added to the ascorbic acid free medium.

For immunocytochemical staining the beating areas of the cell colonies were cut with a scalpel and treated with collagenase A (Roche Diagnostics, Mannheim, Germany). Dissociated cells were plated on 0.1% gelatin-coated 24-well plate wells in KO-DMEM containing 20% FBS. A maximum of seven days after dissociation, beating cells were fixed with 4% paraformaldehyde (PFA, Sigma-Aldrich) for immunostaining with cardiac markers: anti-cardiac-troponin-T (1:1500, Abcam, Cambridge, MA, USA), anti-α-actinin (1:1500, Sigma-Aldrich), anti-myosin-heavy-chain (MHC, 1:100, Millipore), anti-ventricular-myosin-light-chain (MLC2v, 1:150, Abcam) and anti-atrial-myosin-light-chain (MLC2a, 1:300, Abcam). The secondary antibodies were Alexa-Fluor-568-donkey-anti-goat-IgG, Alexa-Fluor-568-goat-anti-mouse-IgG, Alexa-Fluor-488-donkey-anti-rabbit-IgG, and Alexa-Fluor-488-donkey-anti-mouse-IgG (all 1:800, all from Life Technologies Ltd).

2.5. Video recording

For the video recordings CM aggregates were dissociated in the same way as for immunocytochemical analysis (see above). Videos were recorded within a week from dissociation using video microscopy (Nikon Eclipse TS100, Nikon Corporation, Tokyo, Japan) with a video camera Optika DIGI-12 (Optika Microscopes, Ponteranica, Italy). 30–60 second long monochrome videos were recorded with 720 × 480 resolution and 30 frames per second. Beating was determined as normal if the rhythm was regular and the phases of contraction and relaxation followed each other without any delay or additional movement of the cell. Any deviation from that was considered as abnormal beating.

2.6. Beating analysis

In total 58 videos (13 controls, 24 LQT1-G589D (FinA)-specific and 25 LQT1-ivs7-2A>G (FinB)-specific) were analyzed using digital image correlation (DIC) based analysis method, as described by Ahola et al. [22]. In brief, the velocity vector fields representing video image gray level changes in pixel level were calculated from subsequent video frames using a minimum quadratic difference based DIC method. For each CM, the beating focus point was visually determined and the CM was divided into 8 sectors, each comprising of 45° sector, around the beating focus point. With each selection, motion towards the beating focus point was determined as radial, and perpendicular motion as tangential movement. The sum radial and tangential components were computed for each sector.

Out of the 16 possible signals obtained from a CM 3 signals were selected based on the signal quality. From these signals the average parameters of beating were defined: (1) duration of the contraction, (2) time when contracted, (3) duration of the relaxation, (4) incomplete relaxation time and (5) time when relaxed.

2.7. Allelic imbalance

Allelic discrimination between the WT and mutated *KCNQ1* alleles in CMs derived from different iPSC lines was done by qPCR using standard curves. In order to establish a *KCNQ1* allelic standard curves, the plasmid with WT *KCNQ1* and the plasmid containing the mutant allele were combined with following ratios: 1:0, 8:1, 4:1, 2:1, 1:1, 1:2, 1:4, 1:8 and 0:1, respectively, for the qPCR reactions [12]. The standard curves were done similarly for both mutations (G589D and ivs7-2A>G) addressed in this study. Plasmids used for the curve preparation were pBluescript SK+ plasmids (Addgene) with the inserted gene at the BamHI/NotI-site. The standard curves were plotted $\log_2$ of WT/mutant ratios of plasmids *versus* corresponding ΔCt values. The ΔCt values were defined by subtracting Ct value of WT allele from Ct value of the allele with the mutation. In standard curves, ΔCt values for plasmid ratios are represented in statistical form of mean ± standard deviation (n = 3) [18].

In addition, ΔCt values were defined for *KCNQ1* mutations and those were used for locate spots of *KCNQ1* mutated samples on plasmid-derived standard curves. The location of spot defines allelic imbalance of mutation when compared to nearby plasmid ratios.

To determine the allelic imbalance of *KCNQ1* in CMs originated from different mutation specific cell lines (UTA.00208.LQT1 with G589D, and UTA.00118.LQT1 containing ivs7-2A>G) the clusters of beating areas were first cut using a scalpel and total RNA was purified from the cell clusters with a NucleoSpin® RNA II Kit (Macherey-Nagel GmbH & Co.) according to the manufacturer's protocol. The isolated RNA was converted into cDNAs using a High Capacity cDNA Reverse Transcription Kit (Life Technologies Ltd). For allelic discrimination the primers and probes were designed by Custom TaqMan® SNP Genotyping Assay service (Life Technologies Ltd). qPCR reactions were done using 7.5 μl 2× TaqMan® Universal PCR Master Mix, 0.375 μl Custom TaqMan® SNP Genotyping Assay, and 2.125 μl sterile water with total volumes of 12 μl and 3 μl of cDNA or plasmid DNA added into the reaction. The program was initiated with 2 min at 50 °C and 10 min at 95 °C following 40 cycles of 15 s at 95 °C and 1 min at 60 °C.

2.8. Current clamp-measurements

2.8.1. Potassium channel blockers

Rapid delayed rectifying potassium (I_{Kr} or hERG) channel blocker, N-[4-[[1-[2-(6-methyl-2-pyridinyl)ethyl]-4-piperidinyl]carbonyl]phenyl] methanesulfonamide dihydrochloride (E-4031 [24] Sigma-Aldrich) was dissolved in H_2O (stock 2.11 mM) and stored at −20 °C. I_{Ks} blocker, 2-(4-chlorophenoxy)-2-methyl-N-[5 [(methylsulfonyl)amino]tricyclo [3.3.1.13,7]dec-2-yl]-propanamide (JNJ303 [25] Tocris Bioscience, Bristol, United Kingdom) was dissolved in DMSO (stock 25 mM) and stored at −20 °C. Experimental HEPES based perfusate with E-4031 and JNJ303 was freshly prepared on the day of use by dissolving the stocks to final concentrations of 100 nM and 300 nM (DMSO 0.03%), respectively. Action potentials (APs) were unaffected by a 0.03% DMSO vehicle tested in 5/5 CMs.

2.8.2. Measurement of action potentials

APs were recorded from spontaneously beating CMs in current-clamp mode using the perforated patch configuration [26] The HEPES based extracellular perfusate consisted of (in mM): 143 NaCl, 4.8 KCl, 1.8 $CaCl_2$, 1.2 $MgCl_2$, 5 glucose, and 10 HEPES, pH was adjusted to 7.4 with NaOH (at room temperature) and the osmolarity set to 308 ± 2 mOsm with sucrose (Gonotec, Osmomat 030, Labo Line Oy, Helsinki, Finland). The intracellular solution consisted of (in mM): 122 $KMeSO_4$, 30 KCl, 1 $MgCl_2$, and 10 HEPES. KOH was used to set pH to 7.15 and the osmolarity was set to 302 ± 2 mOsm. Amphotericin B (Sigma-Aldrich) was used as a membrane perforation agent and dissolved in DMSO to a final concentration in the patch pipette of 0.24 mg/ml. Dissociation of the spontaneously beating CMs was done similarly as for immunocytochemical staining and for video recordings but the cells were plated onto 0.1% gelatin-coated cover glasses of 5 mmø for patch clamp-measurements. The CMs were recorded on days 6–7 after plating. Coverglasses with CMs were fast transferred to a preheated 36 ± 1 °C fast RC-24N perfusion chamber (Warner Instruments LLC, Hamden, CT, USA). An SH-27B inline heater (Warner Instruments LLC) was used to preheat the perfusate. Cells were rested in the extracellular perfusate for more than 10 min prior to patching. Patch electrodes (model PG150T, Harvard Apparatus, Holliston, MA, USA) were pulled with a PC-10 puller (Narishige International Limited, London, UK) and flame polished with microforge MF-900 (Narishige International Limited) to a resistance of 3.0–3.5 MΩ measured in the bath perfusate. Drugs

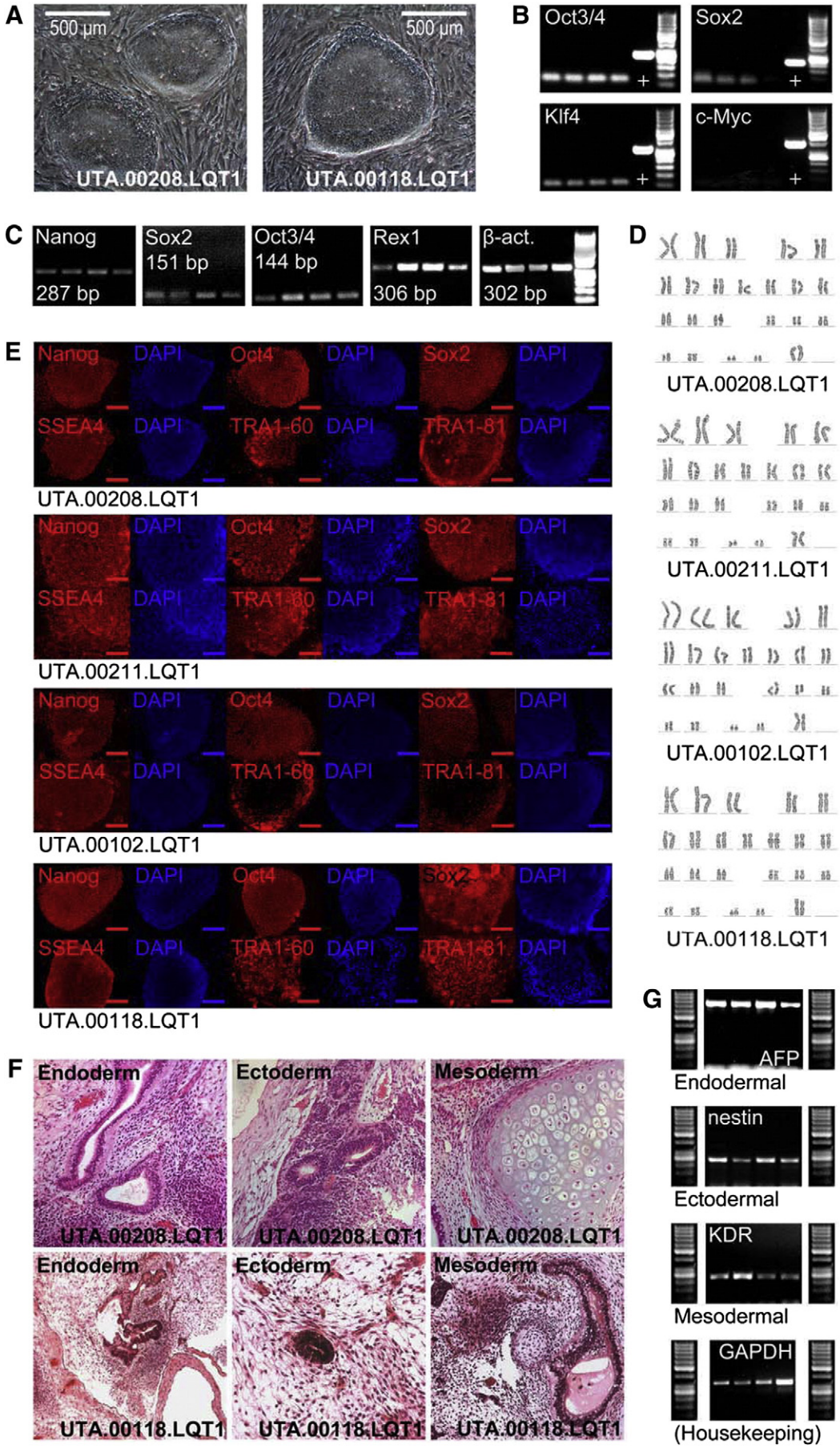
A
500 µm
UTA.00208.LQT1
500 µm
UTA.00118.LQT1
B
Oct3/4
Sox2
Klf4
c-Myc
C
Nanog
287 bp
Sox2
151 bp
Oct3/4
144 bp
Rex1
306 bp
β-act.
302 bp
D
UTA.00208.LQT1
UTA.00211.LQT1
UTA.00102.LQT1
UTA.00118.LQT1
E
Nanog DAPI Oct4 DAPI Sox2 DAPI
SSEA4 DAPI TRA1-60 DAPI TRA1-81 DAPI
UTA.00208.LQT1
UTA.00211.LQT1
UTA.00102.LQT1
UTA.00118.LQT1
F
Endoderm
Ectoderm
Mesoderm
UTA.00208.LQT1
UTA.00118.LQT1
G
AFP
Endodermal
nestin
Ectodermal
KDR
Mesodermal
GAPDH
(Housekeeping)

were applied using a gravity controlled VC3 perfusion system (ALA Scientific Instruments, Farmingdale, NY, USA). APs were recorded in gap-free mode with pClamp 10.2 using the Axopatch 200B patch clamp amplifier connected to an acquisition computer *via* AD/DA Digidata 1440 (Molecular devices LLC). Current-clamp recordings were digitally sampled at 20 kHz and filtered at 5 kHz using the low pass Bessel filter on the recording amplifier. Numbers of CMs measured (n) are presented in the Tables 2A and 2B, and Tables 3A and 3B.

2.8.3. Extraction of action potential characteristics

Following stabilization of the spontaneously generated APs in current-clamp mode, a baseline of minimum of 2 min was acquired before drug application. Gap-free traces of individual CM recordings were then imported into Microcal Origin™ 8.6 or 9.0 and processed by an automated script. Beats per minute (BPM), AP duration at 50% and 90% of repolarization (APD_{50} and APD_{90}), AP amplitude (APA), and maximum diastolic potential (MDP) were extracted. dV/dT (V_{max}, maximal upstroke velocity) was extracted from the differentiated time course traces as peak values corresponding to each single AP. Single AP characteristics were then plotted as a function of time for evaluation and a series of minimum of 15 APs were averaged for each CM and used in the statistical analysis. Ventricular-like CMs were defined by $APD_{90}/APD_{50} < 1.3$ and APA>95 mV, atrial-like by $APD_{90}/APD_{50} > 1.3$ and APA>95 mV and finally nodal-like were defined by $APD_{90}/APD_{50} > 1.3$ and APA < 95 mV.

2.9. Combined current clamp-measurements and video analysis

APs from a CM of each cell line (control, G589D and ivs7-2A>G) were recorded using a current clamp. During the current clamp-measurement, a concurrent video was recorded using an inverted IX71 microscope (Olympus Corporation, Hamburg, Germany) and an ANDOR iXon 885 CCD camera (Andor Technology, Belfast, Northern Ireland). The video recordings were then analyzed using the previously described method [22]. A good quality beating motion signal was selected, and the AP and the motion signal for each cell line were synchronized.

2.10. Calcium imaging

CMs were dissociated as described in the section about immunocytochemical staining and plated onto 0.1% gelatin-coated 13 mm cover slips. 6–8 days after dissociation the cells were loaded with 4 μM Fura-2 AM (Life Technologies Ltd) for 30 min in HEPES based medium at 37 °C. After incubation the cover slips were moved to an RC-25 recording chamber (Warner Instruments LLC) and perfused with 36 ± 1 °C HEPES based solution (in mM): 137 NaCl, 5 KCl, 0.44 KH_2PO_4, 20 HEPES, 4.2 $NaHCO_3$, 5 D-glucose, 2 $CaCl_2$, 1.2 $MgCl_2$ and 1 Na-pyruvate with pH adjusted to 7.4 with NaOH. Ca^{2+}-measurements were done with an inverted IX71 microscope and UApo/340 ×20 air objective (Olympus Corporation). Images were acquired with an ANDOR iXon 885 CCD camera (Andor Technology). A Polychrome V light source (15 nm bandwidth) and the camera were synchronized by an external DSP controller (TILL Photonics, Munich, Germany). TILLvisION software was used to acquire image data (TILL Photonics). Fura-2 in spontaneously beating cells was exited at 340 nm and 380 nm light and emission was detected at 505 nm and the data presented as ratios. The Ca^{2+} handling was extracted for 15 s sweeps of spontaneous baseline beating and categorized into different rhythm categories based on the types of abnormalities observed: normal beating with stable amplitude (N), arrhythmias with double or more Ca^{2+} peaks (AD), and arrhythmias with small amplitude Ca^{2+} events between the stable amplitude Ca^{2+} spikes (AS). A criterion for the AD group was a Ca^{2+} spike with double or several peaks which do not reach the baseline. For the AS group the presence of a small amplitude Ca^{2+} event of at least 10% of the preceding Ca^{2+} spike amplitude was required. Numbers (n) of CMs measured were: for G589D specific cells the n = 87, for 7-2A>G mutated the n = 80, and for control CMs the n = 45.

2.11. Statistical analysis

The variance between two experiments or more was calculated in Microcal Origin™ 9.0. Variance between two individual experiments was accessed using the two sample *t*-test and between more than two individual experiments the one-way ANOVA-test was used and followed by a Scheffe's post hoc-test. In drug experiments, the baseline and drug effect were compared using paired sample *t*-test. $p < 0.05$ was considered significantly different and levels of significance are represented as (*) $p < 0.05$ and (**) $p < 0.01$. Data is shown as mean ± S.E.M. if not otherwise stated.

3. Results

3.1. Pluripotency of the iPSCs

All the iPSC lines used in this study were verified for their pluripotency (control iPSCs have been characterized earlier [22]). Both control and LQT1-specific lines formed colonies typical for human pluripotent stem cells (Fig. 1 A). The iPSCs also expressed markers for pluripotent state shown both by RT-PCT and immunocytochemistry (Fig. 1 C and E), and the transgenes were silenced (Fig. 1 B). *In vitro* pluripotency was shown by embryoid body (EB) formation (Fig. 1 G) and *in vivo* by teratoma forming assay (Fig. 1 F). All the lines were also verified for the normal karyotype (Fig. 1 D).

3.2. Biochemical and genetic analysis of iPSC derived CMs

The expression pattern of spontaneously single beating cells was typical for CMs exhibiting troponin T, α-actinin, myosin heavy chain (MHC), atrial specific myosin light chain (MLC2a) and ventricular myosin light chain (MLC2v). Fig. 2 A–C depicts representative immunostainings of control (Fig. 2 A), G589D (Fig. 2 B) and ivs7-2A>G (Fig. 2 C) specific cell lines.

The LQT1-specific lines were found to carry the correct mutations and these mutations were not found in control lines. This was determined by RT-PCR analysis and restriction enzyme digestion (Fig. 2 D–F).

3.3. Mechanical properties of LQT1-specific CMs

We first visually analyzed the beating behavior of single CMs in videos obtained from the two control lines, the two G589D specific lines and the two ivs7-2A>G specific lines. Control CMs used in the video analysis had a normal beating pattern (marginal irregularities, see below) with only contraction and relaxation phases following each other. However, with our two G589D specific lines we also observed a large proportion of abnormally beating cells with a prolonged phase of contracted state before relaxation. The two ivs7-2A>G lines were also having a prolonged contraction/relaxation cycle. These cells typically had normal contraction but the relaxation phase was prolonged having vacillation before cells fully relaxed (see Supplementary videos 1–3).

Fig. 1. Pluripotency of iPSC lines. A: All the iPSC lines formed colonies typical for pluripotent stem cells. B and C: All the exogenous transgenes (Oct3/4, Sox2, Klf4 and c-Myc) were silenced (B) and endogenous markers for pluripotent state (Nanog, Sox2, Oct3/4 and Rex1) were expressed (C). β-Actin was used as a housekeeping gene. D: All the iPS cell lines had normal karyotype. E: Immunocytochemistry demonstrated the expression of pluripotency markers. F: Cell types derived from all three germ layers were found in teratomas. G: The expression of markers for the three germ layers was detected from EBs by RT-PCR.

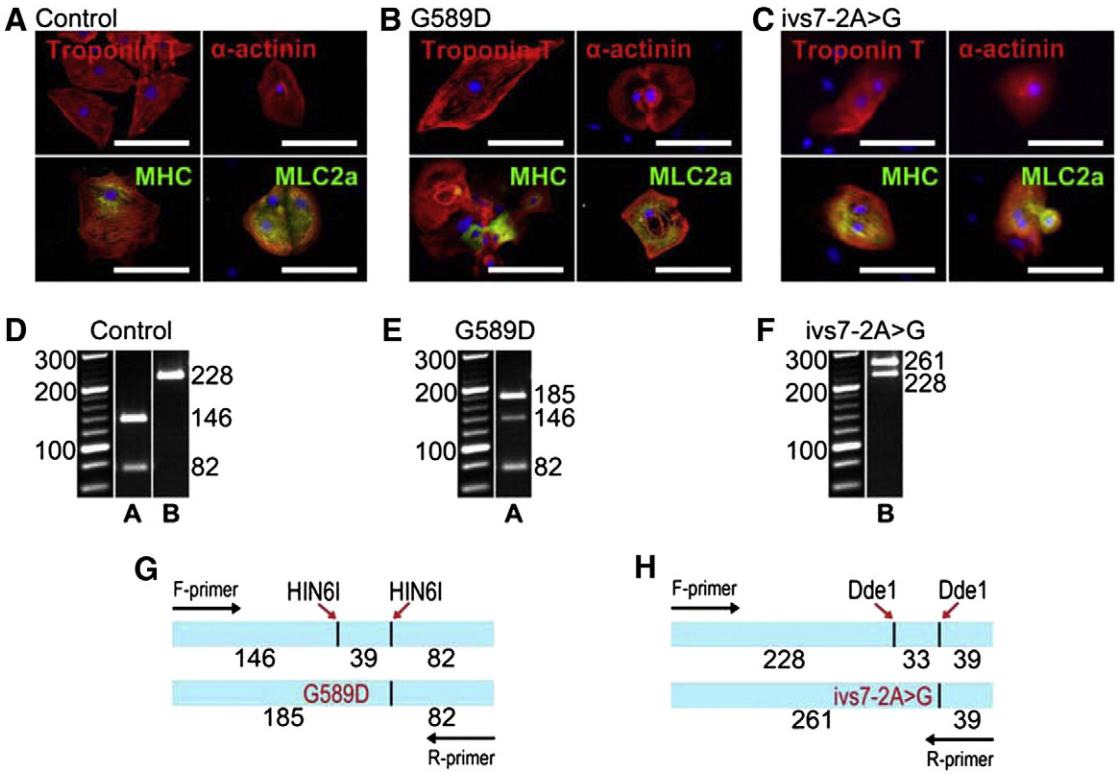

Fig. 2. Characterization of iPSC derived CMs. A–C: The CMs expressed cardiac-specific proteins. The scale bars refer to 100 μm. D–F: The LQT1-specific lines carried the correct mutations while no G589D or ivs7-2A>G mutations were found in control cell lines. "A" in the figure refers to G589D mutation and "B" to ivs7-2A>G. Control CMs produced products of 146 and 82 bp (and 39 bp, not shown in the figure) for G589D, and 228 bp-product (also fragments of 39 and 33 bp, not shown in the figure) for the region corresponding ivs7-2A>G mutation (D). Heterozygous G589D specific lines (one shown in E) created an extra product of 185 bp and heterozygous ivs7-2A>G lines had an extra product with the size of 261 bp (one in F). G and H illustrate the cleavage sites for the restriction enzymes used, their disappearance due to the mutations and the sizes of the products from the reactions for G589D (G) and ivs7-2A>G (H).

Videos from control as well as LQT1-CMs with either of the mutations were analyzed in detail according to the displacement model illustrated in Fig. 4 A (see also the Methods section). Representative signals from single CMs from both LQT1-specific cell lines (G589D or ivs7-2A>G) as well as from control CM are presented in Fig. 3 D–F. Normally beating control CMs (n = 13) comprised only of the phases 1 (contraction), 3 (relaxation) and 5 (relaxed) (Fig. 4 B). However, in 17/24 CMs with G589D mutation, a prolonged contraction time was observed: They exhibited an additional phase 2 between contraction and relaxation phases, and during that phase the CMs stayed contracted. In a minor proportion (2/17) of G589D-CMs, a phase 4 (incomplete relaxation) was also found (Table 1, Fig. 4 C). CMs carrying the ivs7-2A>G mutation also exhibited a prolonged contraction (phase 2, in 17/25), but the duration of the phase 2 was not as prominent as in G589D-CMs. Instead, ivs7-2A>G-CMs typically had rather normal contraction, but the relaxation was abnormal and prolonged (in 15/17 CMs) due to vacillation (incomplete relaxation, phase 4, Table 1, Fig. 4 D). The time durations of different phases in control CMs and in CMs with the two LQT1 specific mutations are summarized in Table 1. There was some overlap in the abnormal beating behavior between the two mutations: However, only 12% (2/17) of the cells with G589D failed to relax normally, but 88% (15/17) of the cells with ivs7-2A>G demonstrated some prolongation in the contraction phase (phase 2). Beating patterns comparable to controls were also observed in CMs with G589D (n = 7/24, 29%) or ivs7-2A>G (n = 8/25, 32%).

When the absolute time of contraction (phases 1 and 2), relaxation (phases 3 and 5) and incomplete relaxation (phase 4) was plotted against the beating frequency the contraction time for the control cell population (Fig. 4 E) stayed at the range of 0.25–0.5 s corresponding the contraction time of human heart [27]. The relaxation time increased with a decreased beating rate also resembling the behavior of human heart. The abnormally beating LQT1-CMs presented contraction times of up to 0.75 s, while the contraction times of the control cells were less than 0.5 s (a not statistically significant difference, one-way ANOVA). If incomplete relaxation (phase 4) was added to the contraction time, the total times when the cells were not relaxed, were even more different from the times observed in normally beating cells although the difference was still not statistically significant (Fig. 4 F and G). The normally beating LQT1-CMs resembled control CMs regarding their contraction-relaxation properties (Supplementary Fig. 1).

3.4. Allelic imbalance in patient specific cells

The allelic discriminations between the WT and mutated *KCNQ1* alleles in CMs specific for either G589D or ivs7-2A>G mutation were determined. The expression ratio between the WT and the G589D-*KCNQ1* was found to be 4:1 (WT:mutated) in both LQT1-G589D cell lines (Supplementary Fig. 2). For the *KCNQ1*-ivs7-2A>G mutation the discovered ratio was 3:1 (WT:mutated) (Supplementary Fig. 2).

3.5. Electrical properties of LQTS-specific CMs

3.5.1. Baseline characteristics

Representative APs from ventricular CMs (both G589D and ivs7-2A>G-specific) as well as from control CM are presented in Fig. 3 G–I. The majority of the CMs recorded were ventricular-like and only a marginal proportion was nodal-like (Table 2A). As expected, the APDs were significantly prolonged in nodal-, atrial- and ventricular-like LQT1-CMs compared to the control CMs (Fig. 5 D, ANOVA, $p < 0.05$). MDPs for atrial- and ventricular-like CMs were recorded from −65 mV to −82 mV with overshoots of around +40 mV. In contrast, nodal-like CMs were more depolarized and around −66 mV with overshoots less than +25 mV (Table 2A).

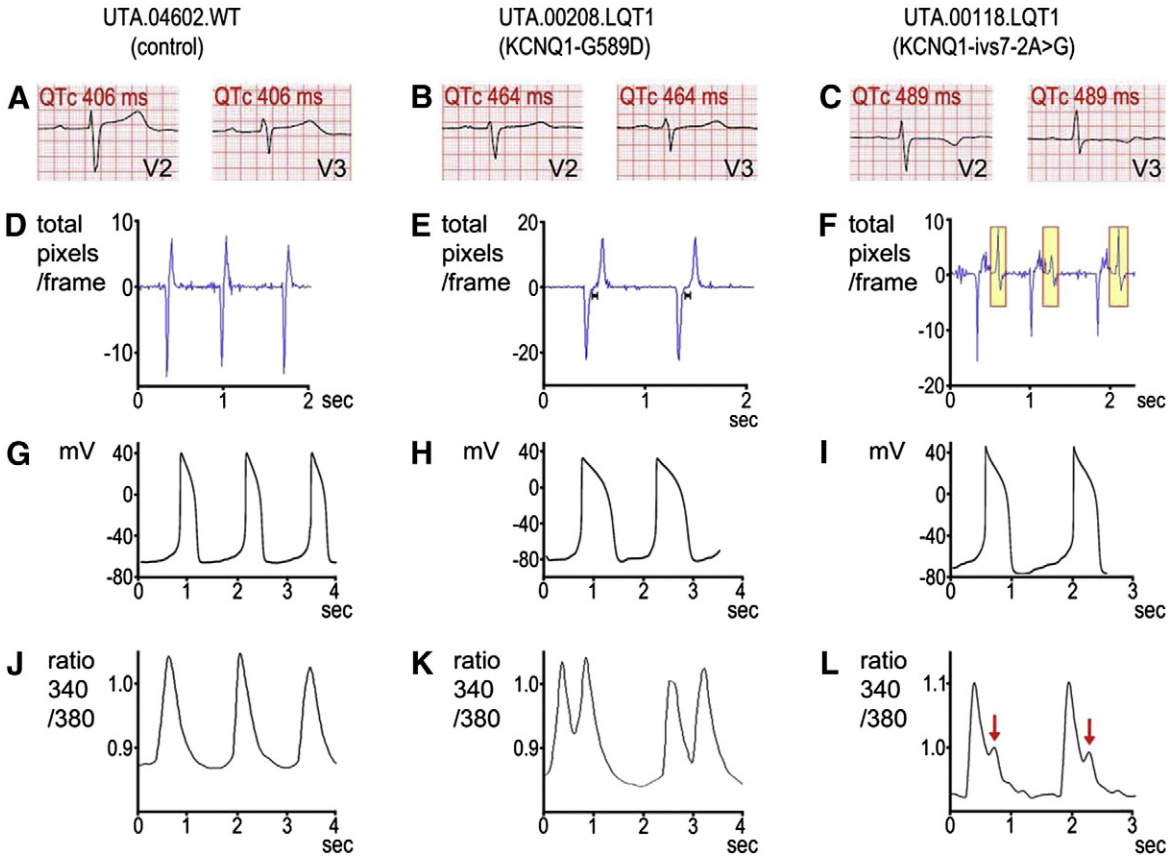

Fig. 3. ECGs of the donors and functionality of iPSC derived CMs. A–C: ECGs from the primary cell donors. D–F: Video recording analysis of control (D), G589D (E) and ivs7-2A>G (F)-specific CMs. Contraction is indicated with downward peak and the upward peak refers to relaxation. Bars (E) indicate the phase 2 (see Fig. 4 A) and show the time when the CMs stayed contracted and the highlighted areas (F) refer to the time of incomplete relaxation (phase 4 in Fig. 4 A). G–I: Ventricular APs from control CMs (G) and LQT1-specific CMs carrying G589D (H) or ivs7-2A>G (I). J–L: Ca^{2+}-imaging signals from control (J) and LQT1-specific CMs (K, L). The most prevalent type of abnormal Ca^{2+} transients in ivs7-2A>G-specific CMs was additional small Ca^{2+} transients (AS) (L, extra peaks marked with arrows) but in G589D CMs double or more Ca^{2+} peaks (AD) (K) in addition to AS were seen.

In the G589D-specific CMs, but not in controls or in ivs7-2A>G-specific CMs, spontaneous baseline early afterdepolarizations (EADs) were observed in 16.7% (5/30) of ventricular-like CMs (Fig. 5 E, Table 2B). These CMs with baseline EADs were not used in the drug studies. Nevertheless, in these cells with spontaneous EADs we found a consistent elevation of the APD_{90}/APD_{50} ratios (>1.8) compared to baseline ratios without EADs (<1.3). The ratio prolongation is due to the presence of EADs evoking around −25 mV, and thereby prolonging only the APD_{90} value (see Fig. 5 E).

3.5.2. Effect of JNJ303 and E-4031

Ventricular-like CMs were exposed to the I_{Ks} blocker, JNJ303 (300 nM) and APs from the baseline, in the presence of JNJ303 and after wash out was extracted (Fig. 5 F). In control CMs (n = 10), JNJ303 significantly prolonged APD_{50} and APD_{90} by a similar proportion of 31% and 28%, respectively, but other AP characteristics were unaffected (Table 3A). However, the effect of JNJ303 was only marginal on the APD_{50} and APD_{90} in G589D-specific cells (prolongation of 7.7% and 8.7%, respectively, Fig. 5 F, middle panel), and in ivs7-2A>G-specific CMs no effects were observed (Table 3A, Fig. 5 F, lower panel). The effect of JNJ303 was fully reversible following the wash out, and the beating frequency was not significantly affected. In a few cells from each group the JNJ303 block was verified by a consecutive application, which always was similar to the first (Fig. 5 F, LQT1-G589D). The APD_{90}/APD_{50} ratios for the control, G589D-specific- and ivs7-2A>G-specific CMs at baselines and in the presence of JNJ303 were similar and found to be between 1.19–1.27.

To evaluate our I_{Ks} findings we also applied the I_{Kr} (hERG) blocker, E-4031 (100 nM) on ventricular-like CMs. The effect of E-4031 from three representative current-clamp recordings is shown in Fig. 5 G. In control cells the APD_{50} and APD_{90} were prolonged by E-4031 (30% and 74%, respectively), and the APD_{90}/APD_{50} ratio was now increased from 1.21 (baseline) to 1.67 (E-4031) but no EADs were evoked (Fig. 5 G, upper panel, Table 3B). In contrast, all ventricular-like CMs in the G589D-specific group (5 cells) and in the ivs7-2A>G-specific group (7 cells) exhibited EADs when exposed to E-4031 (Fig. 5 G, middle and lower panel, respectively). The G589D-CMs had APD_{50} and APD_{90} significantly prolonged by 70% and 318% (paired sample *t*-test), respectively, and ADP_{90}/APD_{50} ratios were found to be increased from 1.16 (baseline) to 2.18 (E-4031). In the CMs with ivs7-2A>G, APD_{50} and APD_{90} were even more significantly prolonged by 412% and 771% (paired sample *t*-test), respectively, and ADP_{90}/APD_{50} ratios were found to be increased from 1.14 (baseline) to 2.09 (E-4031). In contrast to the effects of JNJ303, E-4031 decreased the beating frequency of all CMs (paired sample *t*-test). All CMs tested with E-4031 became significantly depolarized during exposure (paired sample *t*-test), but the overshoot (peak) was not affected by E-4031 (Fig. 5 G, Table 3B). Even though APDs nearly recovered following wash out the, MDPs recovered only partially (Fig. 5 G, right panels) after exposure to E-4031. In line with this, the beating frequency increased following the wash out (data not shown).

3.6. Comparison of the electrical and mechanical phenotypes

The mechanical analysis was also conducted together with the current clamp-measurements (Fig. 6). Thereby the mechanical and electrophysiological phenotypes could be compared and the timing of the electrical activity and the contraction/relaxation of the cells could be evaluated. In both cell types, control CMs (Fig. 6 A) and LQT1 specific

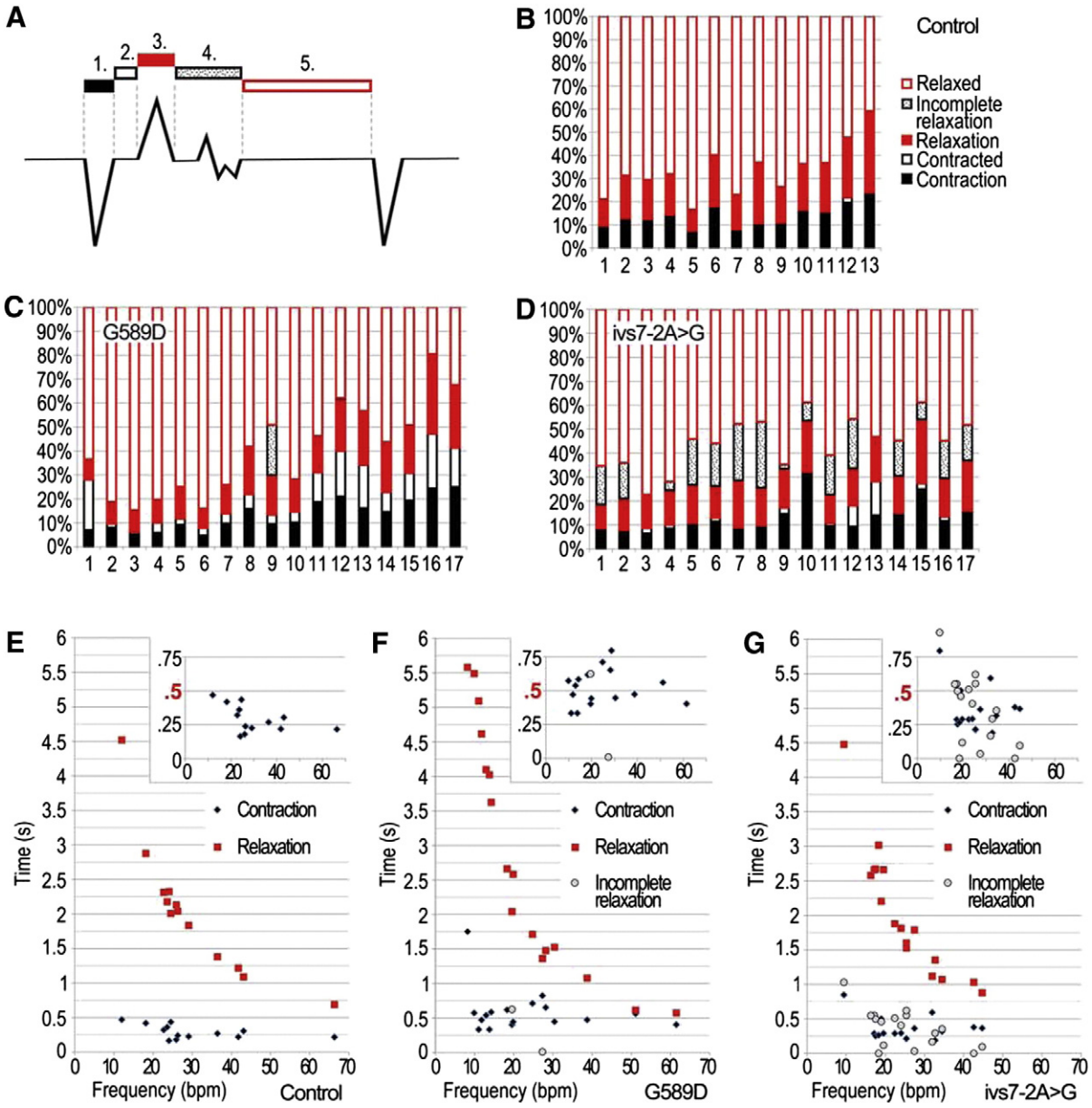

Fig. 4. Analysis of LQT1-CMs using digital image correlation. A: An artificial illustration of a beating signal. 1: time of contraction (phase 1), 2: time in contracted state (phase 2), 3: time of relaxation (phase 3), 4: time of incomplete relaxation (phase 4), and 5: time in relaxed state (phase 5) (see phases also in Table 1). The same colors and patterns are used in panels B–G. B: Beating pattern of control CMs. C: Beating pattern of G589D-CMs. D: Beating pattern of ivs7-2A>G-CMs. The cells are presented in order of beating rate: control CMs: 12–66 beats/min, G589D-CMs: 8–62 beats/min and ivs7-2A>G-CMs: 9–45 beats/min. E–G: The time duration from the beginning of contraction to the beginning of relaxation and from the beginning of relaxation to the beginning of contraction are presented. Contraction time was in the range of 0.25–0.5 s in control CMs (E). In LQT1-CMs the contraction time was longer or incomplete relaxation was present (F and G). The points for contraction time are enlarged to highlight the differences in the contraction times between control CMs and LQT1 specific CMs (a point with a value of 1.75 ms in G589D-figure is not included).

CMs (Fig. 6 B), the AP was immediately followed by the contraction. In LQT1 specific CMs the APD was clearly prolonged and the mechanical abnormality correlated nicely with this prolongation (Fig. 6 B). Also, the mechanical activity of the LQT1 specific cells seemed to continue longer after the electrical activity had already stopped when compared to control CMs.

3.7. Ca^{2+} handling of LQT1-specific CMs

To further study the functionality of LQT1 specific CMs, Ca^{2+} transients were measured during spontaneous baseline beating. In G589D and ivs7-2A>G specific as well as in controls three major responses were found. A robust beating pattern with stable Ca^{2+} amplitude and frequency were characteristic for the majority of the control CMs (N), while arrhythmias with double or more Ca^{2+} peaks (AD) or arrhythmias with small amplitude Ca^{2+} events between the stable amplitude Ca^{2+} spikes (AS) were frequently seen in G589D and ivs7-2A>G CMs (Fig. 7 A, Supplementary Table 1). Both types of arrhythmias (AD and AS) were seen in all cell types though the Ca^{2+} transient abnormalities were more prevalent in both LQT1 specific cell lines compared to control CMs (Fig. 7 B). The cells with G589D had the highest proportion of ADs (23%). The duration of the calcium elevation was significantly longer in CMs with G589D exhibiting ADs compared to those showing AS type of arrhythmia or normal beating ($p < 0.01$, one-way ANOVA). AS-arrhythmia were also more pronounced in CMs with G589D resulting in significantly lower beating frequency ($p < 0.02$, one-way ANOVA).

Table 1
The average times (ms) and standard mean errors for each individual beating phase and the total sum of the phases. Phase 1 is the time of contraction, phase 2 refers to the time when the cells stay contracted, phase 3 is the relaxation time, and phase 4 indicates the time of incomplete relaxation. The time when the cells are relaxed (phase 5) is not displayed in the table. (*) indicates $p < 0.05$ and (***) indicates $p < 0.001$ (one-way ANOVA) for abnormal G589D-CMs vs. control CMs and vs. abnormal ivs7-2A>G-CMs concerning the phase 2. For abnormal ivs7-2A>G-CMs vs. abnormal G589D-CMs (two sample t-test) in the case of the phase 4 (*) also indicates $p < 0.05$ and (***) indicates $p < 0.001$. Data is presented as mean ± S.E.M. The abnormal behavior of the cells is highlighted with bold.

	BPM	Phase 1	Phase 2	Phase 3	Phase 4	Sum P 1–4
Control						
Normal n = 11	29.3 ± 4.4**	294.3 ± 31.9	4.7 ± 1.9	426.0 ± 41.9	N/A	725.0 ± 70.2
Abnormal n = 0	N/A	N/A	N/A	N/A	N/A	N/A
G589D						
Normal n = 7	33.2 ± 6.5	275.9 ± 19.2	15.5 ± 5.7	362.0 ± 19.3	0.0 ± 0	653.4 ± 27.5
Abnormal n = 17	23.6 ± 3.6	285.2 ± 26.3	**180.8 ± 28.8*** (n = 17/17)	365.1 ± 29.1	**37.3 ± 36.7** (n = 2/17)	868 ± 74.8
ivs7-2A>G						
Normal n = 8	30.6 ± 5.7	248.2 ± 31.1	5.0 ± 2.9	383.0 ± 48.0	0.0 ± 0	636.3 ± 79.0
Abnormal n = 17	25.2 ± 2.3	318.7 ± 39.9	**46.3 ± 13.6** (n = 15/17)	424.8 ± 44.4	**366.7 ± 66.9***** (n = 17/17)	1156.4 ± 123.0

Representative Ca^{2+} signals from single CMs from both LQT1-specific cell lines (G589D or ivs7-2A>G) as well as from control CM are shown in Fig. 3 J–L.

4. Discussion

In the present study we analyzed LQT1-specific CMs carrying either G589D or ivs7-2A>G mutation in the *KCNQ1* gene. The LQT1-CMs with either mutation had prolonged AP durations. EADs were spontaneously present only in CMs with G589D mutation but not with ivs7-2A>G mutation. However, EADs could be evoked pharmacologically in CMs with either mutation. In control CMs EADs were absent at baseline and they could not be induced with I_{Ks} or I_{Kr} blockers. Ca^{2+} transients were also aberrant in both types (G589D and ivs7-2A>G) of LQT1-CMs having large double spikes or extra spikes with small amplitude. In control CMs contraction and relaxation happened fast with no pause in-between. However, this beating behavior in LQT1-CMs was clearly abnormal. Using video recording analysis, LQT1-specific CMs were found to exhibit two distinct forms of abnormal mechanical beating behavior: CMs carrying G589D mutation typically stayed contracted for prolonged time while CMs with ivs7-2A>G mutation showed an incomplete relaxation phase.

Our current clamp data demonstrates that the APDs measured from LQT1-CMs with either of the mutations (G589D or ivs7-2A>G) were significantly prolonged. Heterozygous expression of the G589D and ivs7-2A>G mutations in non-cardiac cells has earlier shown that both mutations have a dominant negative effect in gene expression systems [7,28], although the expression of G589D mutation did not lead to altered current density, the cAMP induced up-regulation of I_{Ks} was abolished by the mutation [28]. The ivs7-2A>G mutation on the other hand, almost completely abolished the I_{Ks} current when transiently expressed in non-cardiac cells [7]. The lack of I_{Ks} reduction in the G589D transfected non-cardiac cells may be due to trafficking problems caused by G589D: the mutated protein does not reach the cell surface [9]. The effect of G589D in LQTS has also been explained by disrupted β-adrenergic activation of I_{Ks} [29] but this study clearly shows that the disease phenotype caused by G589D is not solely dependent on central nervous system and activation of β-adrenergic receptor since it is present also in single dissociated CMs.

As mentioned, baseline-APDs were significantly prolonged in LQT1-CMs compared to the control CMs. With LQT1-CM we could further detect that ventricular-like CMs were only marginally affected or completely unaffected by I_{Ks} blockage. The lack of effect of I_{Ks} blockade in our LQT1-CMs is in accordance with the previous observation that the baseline I_{Ks} current is decreased by about 75% in LQT1-CMs [18]. In our study, G589D-CMs had longer baseline-APD_{90} than ivs7-2A>G-CMs and spontaneous EADs were observed only in G589D-CMs, but none in CMs with ivs7-2A>G nor in control CMs. However, the APD prolongation with I_{Kr} blockage always evoked EADs in both types of LQT1-specific CMs but not in control CMs. The I_{Kr} block also induced a depolarization of the baseline as previously shown [30].

CMs carrying either one of the LQT1 mutations demonstrated abnormalities in intracellular Ca^{2+} transients, but the abnormal features were more common in G589D mutated CMs similarly as these CMs had more severe abnormalities in current clamp analysis. Abnormal Ca^{2+} transients could be occasionally observed also in control CMs (6% of the cells), but at least third of the LQT1-CMs presented Ca^{2+} abnormalities. In LQTS-CMs, EADs have been thought to result from late membrane-

Table 2A
Baseline characteristics of spontaneous action potentials (APs) from control cardiomyocytes (CMs) as well as from LQT1-G589D- and LQT1-ivs7-2A>G-specific CMs. (*) indicates significance levels of $p < 0.05$ and (**) $p < 0.01$. Significance levels were obtained by one-way ANOVA of grouped data from nodal, atrial and ventricular CMs, respectively. Data is presented as mean ± S.E.M. CMs with baseline arrhythmia are not included (see Table 2B).

	Number of cells [n (%)]	BPM	APD_{50} (ms)	APD_{90} (ms)	APA (mV)	MDP (mV)	V_{max} (dV/dT)
Control							
Nodal-like	2 (6.7)	75.7 ± 4.4	104.4 ± 2.1	159.1 ± 0.4	88.7 ± 0.6	−66.0 ± 0.3	8.70 ± 2.3
Atrial-like	4 (13.3)	61.5 ± 8.5	132.6 ± 13.6	189.1 ± 32.2	100.4 ± 3.0	−71.6 ± 3.4	26.1 ± 17.9
Ventricular-like	24 (80.0)	55.6 ± 3.4	291.8 ± 21.5	349.6 ± 22.9	110.2 ± 2.4	−69.6 ± 1.5	19.5 ± 4.7
LQT1 (G589D)							
Nodal-like	2 (5.1)	54.5 ± 4.1	164.5 ± 6.2*	309.2 ± 39.7*	83.4 ± 3.7	−63.6 ± 1.7	4.2 ± 7.1
Atrial-like	12 (30.8)	38.9 ± 4.5	335.7 ± 36.2**	477.7 ± 51.4**	106.4 ± 2.8	−70.5 ± 2.0	23.9 ± 6.9
Ventricular-like	25 (64.1)	37.7 ± 4.6*	458.5 ± 57.4**	545.3 ± 62.6**	109.0 ± 3.1	−73.6 ± 1.6	14.8 ± 1.8
LQT1 (ivs7-2A>G)							
Nodal-like	2 (6.1)	69.4 ± 6.0	170.5 ± 17.3	232.1 ± 7.7*	93.0 ± 1.3	−61.0 ± 9.6	9.5 ± 1.5
Atrial-like	6 (18.2)	50.9 ± 9.9	187.8 ± 15.0*	287.8 ± 18.5*	101.2 ± 2.2	−66.0 ± 2.6	16.3 ± 4.2
Ventricular-like	25 (75.7)	45.6 ± 2.8*	416.1 ± 22.1**	481.5 ± 23.6**	115.1 ± 1.3	−72.3 ± 1.0	16.2 ± 2.4

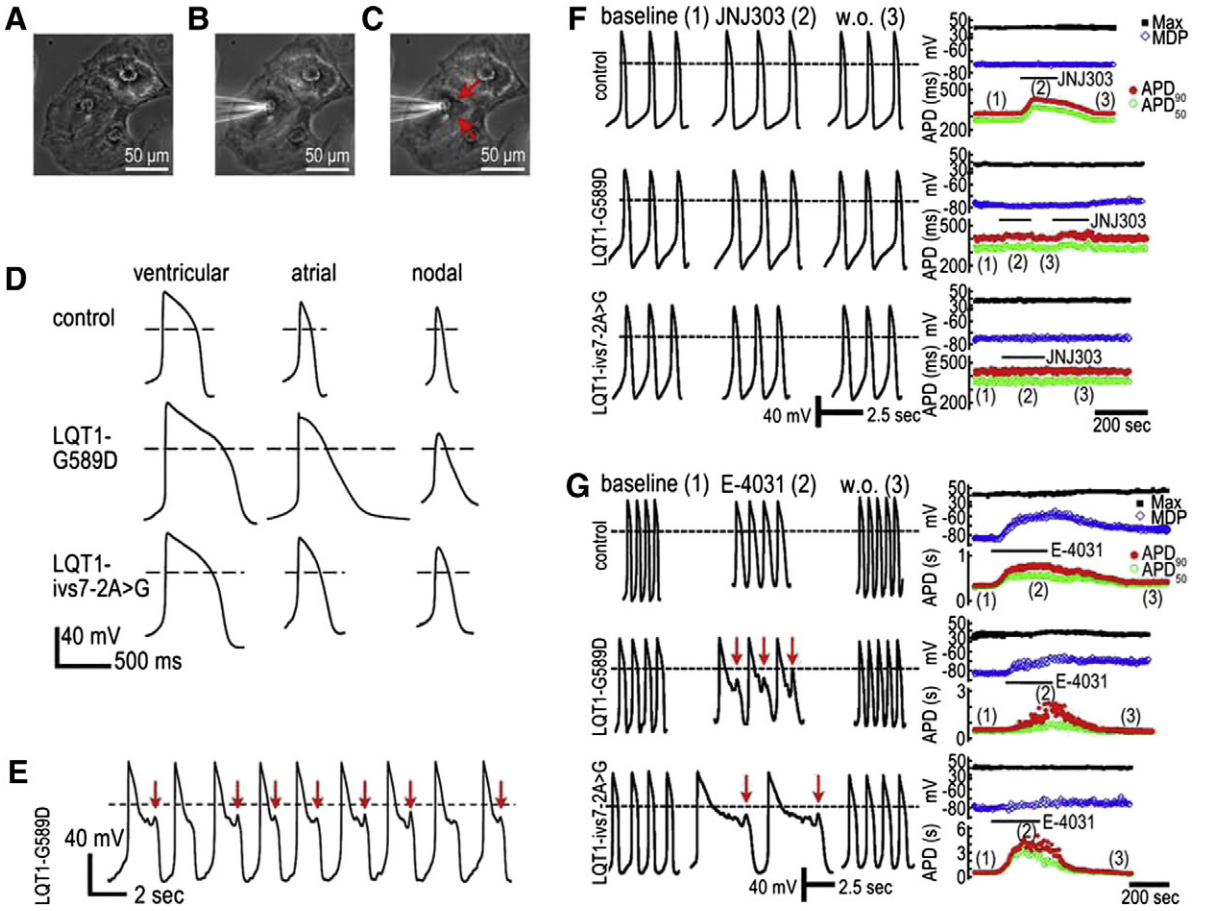

Fig. 5. Current clamp-recordings from control and LQT1-CMs carrying either G589D or ivs7-2A>G. Beating CMs un-patched (A), patched in relaxed phase (B), and patched in contracted phase (C). Arrows indicate the positions where the contraction can be seen (C). D: Current clamp-recordings of ventricular-, atrial- and nodal-like APs are depicted for control (upper panel), G589D (middle panel) and ivs7-2A>G (lower panel)-CMs. E: Baseline characteristics of spontaneous APs with early after depolarizations (EADs) in G589D-specific CMs: dashed line represents 0 mV and arrows indicate EADs. The effects of JNJ303 (F), and E-4031 (G) are shown for ventricular-like AP recordings from controls, as well as from G589D and ivs7-2A>G-CMs. Baseline (1), (2) effect of I_{Ks} (JNJ303) or I_{Ks} (E-4031) blocker, and (3) wash out measurement which fully recovers the effect of JNJ303 but only partially reverses the baseline AP characteristics after the E-4031 treatment. Arrows indicate EADs. The right panels show the time courses for the overshoot (Max), MDP, APD_{90} and APD_{50}. Marks (1), (2) and (3) indicate the times of AP extraction, and the bar represents the exposure of the cells for JNJ303 or E-4031.

Table 2B
Baseline characteristics for G589D-CMs with EADs. Data is presented as mean ± S.E.M.

	Number of cells (n)	BPM	APD_{50} (ms)	APD_{90} (ms)	APA (mV)	MDP (mV)	V_{max} (dV/dT)
LQT1 (G589D)							
Ventricular-like	5	30.1 ± 4.4	820.3 ± 93.1	1559.6 ± 407.1	112.8 ± 3.8	−71.5 ± 2.7	12.7 ± 2.3

inward currents, such as the spontaneous reactivation of the L-type Ca^{2+}-channel during prolonged action potential duration [31]. Therefore it can be assumed that abnormalities in Ca^{2+} transients shown in this study may correspond to EADs and lead to severe arrhythmias. A similar finding has been also earlier observed and demonstrated combining patch clamp and Ca^{2+}-imaging methods [32]. Further studies

Table 3A
Effect of I_{Ks} block on ventricular-like cardiomyocytes (CMs). Statistical difference of *paired sample t-test* is indicated by (*) $p < 0.05$ and (**) $p < 0.01$. Data is presented as mean ± S.E.M.

	Number of cells (n)	BPM	APD_{50} (ms)	APD_{90} (ms)	APA (mV)	MDP (mV)	V_{max} (dV/dT)
Control							
Baseline	10	48.3 ± 8.4	264.7 ± 47.0	334.0 ± 30.1	103.6 ± 3.9	−69.0 ± 2.5	25.3 ± 10.4
300 nM JNJ303		42.8 ± 7.6*	346.6 ± 68.0**	428.2 ± 79.9**	106.3 ± 4.6	−69.7 ± 2.6	27.8 ± 12.3
LQT1 (G589D)							
Baseline	9	44.7 ± 5.5	393.0 ± 57.8	500.4 ± 76.0	108.3 ± 3.1	−71.9 ± 2.6	11.6 ± 2.6
300 nM JNJ303		38.7 ± 5.2	423.6 ± 64.4	544.0 ± 86.0	106.9 ± 2.8	−70.8 ± 2.3	10.9 ± 2.1
LQT1 (ivs7-2A>G)							
Baseline	6	44.5 ± 3.2	387.0 ± 49.3	458.1 ± 51.6	112.4 ± 4.2	−74.2 ± 2.6	9.8 ± 1.9
300 nM JNJ303		43.1 ± 4.6	386.0 ± 36.0	452.0 ± 37.9	111.1 ± 3.6	−72.0 ± 3.1	9.8 ± 1.9

Table 3B
Effect of I_{Kr} block on ventricular-like CMs. Ventricular-like LQT1-specific CMs all showed early after-depolarizations (EADs) in the presence of E-4031. Statistical difference of *paired sample t-test* is indicated by (*) $p < 0.05$, (**) $p < 0.01$ and (***) $p < 0.001$. Data is presented as mean ± S.E.M.

	Number of cells (n)	BPM	APD_{50} (ms)	APD_{90} (ms)	APA (mV)	MDP (mV)	V_{max} (dV/dT)
Control −EADs							
Baseline	5	68.8 ± 4.3	256.8 ± 30.4	308.0 ± 30.1	111.4 ± 3.5	−74.6 ± 3.6	10.1 ± 1.4
100 nM E-4031		60.2 ± 7.6	332.4 ± 82.5	535.3 ± 102.9*	83.3 ± 7.5**	−52.1 ± 1.5**	6.2 ± 1.8
LQT1 (G589D) + EADs							
Baseline	5	43.2 ± 3.5	458.6 ± 25.1	536.0 ± 33.8	114.6 ± 0.4	−81.1 ± 0.9	13.7 ± 2.9
100 nM E-4031		23.5 ± 4.4*	781.7 ± 16.2***	1703.8 ± 100.8**	103.6 ± 1.7*	−70.7 ± 2.9*	9.3 ± 1.5*
LQT1 (ivs7-2A>G) + EADs							
Baseline	7	42.5 ± 3.4	464.7 ± 49.3	526.1 ± 53.6	117.5 ± 1.4	−73.6 ± 1.8	14.1 ± 0.9
100 nM E-4031		13.8 ± 2.6***	1915.7 ± 468.8*	4055.8 ± 1173.1*	109.7 ± 2.6**	−64.1 ± 2.7**	11.3 ± 1.0**

are needed to clarify the mechanism of the different Ca^{2+} transients observed in our study and their correlation with the EADs as well as with the motion abnormalities observed with the two different LQT1 related mutations.

In addition to conventional methods (patch clamp and Ca^{2+}-imaging), we also analyzed the mechanical beating behavior of single LQT1-specific CMs by video imaging and this analysis revealed either prolonged contraction (G589D) or disturbed relaxation (ivs7-2A>G) of the cells. This abnormality has not been reported earlier in iPSC-derived LQTS specific CMs, but the observation is in line with a clinical observation of prolonged contraction duration in LQTS mutation carriers compared to healthy individuals [33]. In this study, combined current clamp-measurements and video analysis of the mechanical behavior demonstrated the correlation between the prolonged APD and abnormal mechanical phenotype also in single LQT1 specific CMs.

The two patients of this study are both heterozygous for the LQT1-mutations and the allelic discrimination study revealed an imbalance in the expression of the WT and mutated forms of *KCNQ1*. The ratio of expression (WT:mutated) for G589D was found to be 4:1 and for ivs7-2A>G the ratio was 3:1. It was reported earlier that LQT1-CMs with R190Q mutation exhibited equal expression of wild type and mutant alleles [18]. With the expression ratios observed in our study, the probability that one or more mutated α-subunits are participating in forming the tetrameric I_{Ks} channel is about 70%. This is in accordance with the functional abnormalities observed in the videos recorded from our CMs. Ca^{2+}-imaging also revealed abnormal Ca^{2+} transients in LQT1 CMs but the proportions of abnormal CMs were slightly lower than those obtained with video imaging. The presence of spontaneous EADs were, however, considerably lower than other abnormalities. It is possible that there are compensatory mechanisms involved in

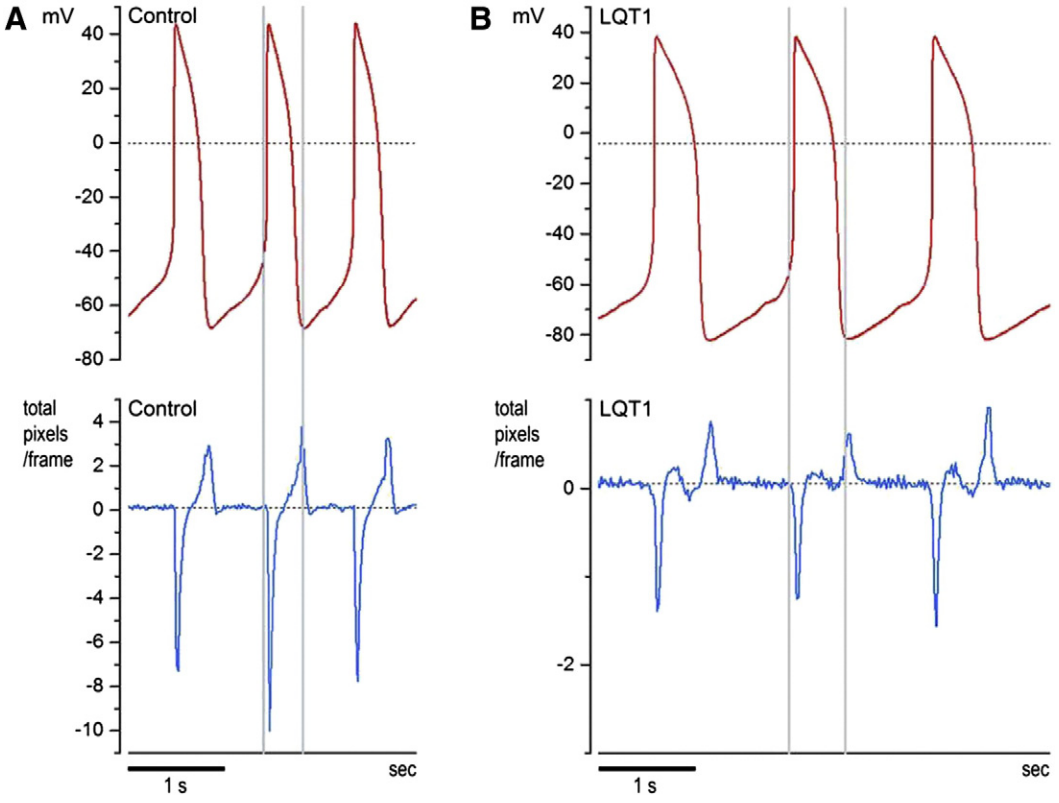

Fig. 6. Combined current clamp-measurements and video analysis. Control CMs (A) as well as the LQT1 specific CMs (B) showed a nice correlation in timing of the contraction and the AP: Contraction followed immediately after the initiation of AP. In LQT1 specific CMs the APD was clearly prolonged compared to the control cells and the mechanical abnormality observed by video analysis correlated with the prolongation of the APD (B).

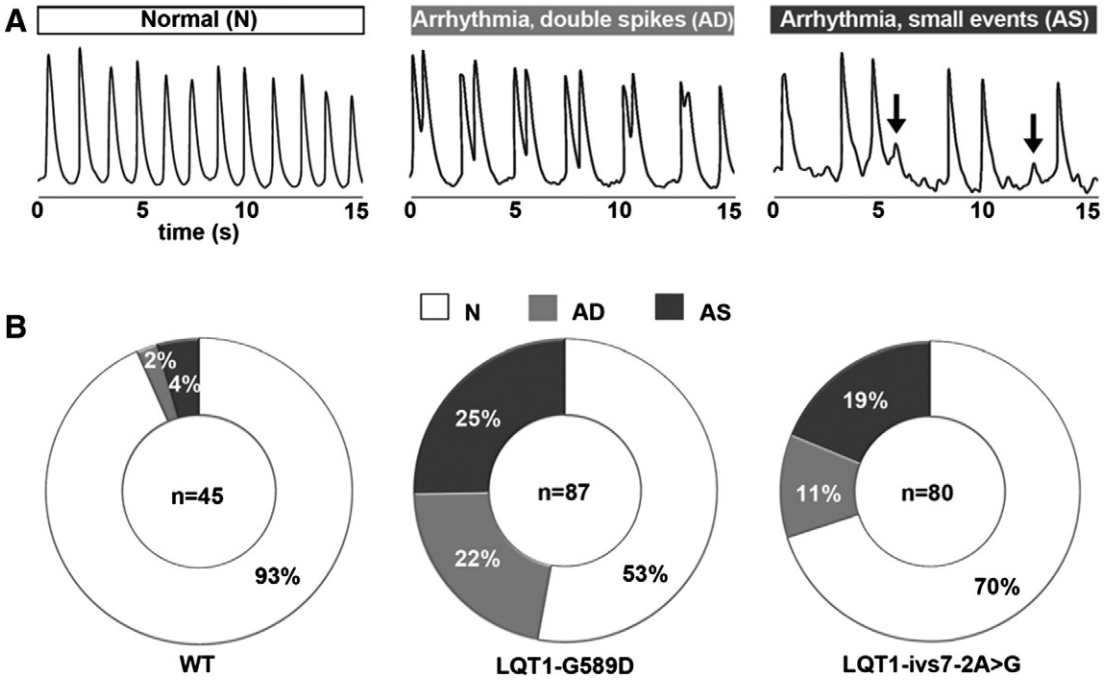

Fig. 7. Analysis of Ca^{2+} transients of control and LQT1 specific CMs. (A) Three different transient categories: normal transients with stable amplitude (N), arrhythmias with double or more Ca^{2+} peaks (AD), and small amplitude Ca^{2+} events (arrows) (AS) were found. (B) Doughnut charts indicate the percentage of the control and LQT1 specific CMs under each transient category (N, AD and AS).

electrical data obtained by patch clamp, resulting in a lower frequency of abnormalities compared to other methods. It is also important to point out that the ratios obtained by allelic imbalance measurements reflect the situation at mRNA level and do not accurately depict the proportions of the two alleles expressed at protein level since the transcripts may be alternatively processed before translation into proteins. Further, there is a possibility that the expression ratio of the WT and mutated allele may vary from cell to cell. It is also possible that the cells with different beating properties could represent also a particular CM subpopulation (ventricular, atrial or nodal).

Our findings support the previous studies [4,6] suggesting that mutations in different parts of the *KCNQ1* gene are associated with different clinical outcomes. However, no clinically distinct differences between the patient groups carrying the two mutations presented in this study have been reported. QTc of G589D-carriers has been reported to be 462 ± 38 if recorded from patients without any medication at the time of ECG recording. For the ivs7-2A>G the corresponding QTc value has been reported to be 470 ± 31 [21]. Both patients investigated here were symptomatic. G589D-patient, 46-year-old female has been suffering from syncopal spells. The other patient, 51-year-old female carrying ivs7-2A>G in *KCNQ1*, has suffered from dizziness, darkening of vision and more recently also from episodes of unconsciousness. On cell level G589D-CMs demonstrated more severely prolonged APDs which could be visualized as prolonged contracted state in beating CMs. The ivs7-2A>G-CMs had less severe APD prolongation at baseline, but they were more sensitive to agents blocking other ion channels. Additionally their beating behavior presented problems in relaxation phase suggesting other, currently unknown problems in repolarization currents in these cells. Since the patients present clinically similar phenotypes, it is most likely that there are some compensatory elements influencing the intact heart which moderate the clinical outcome. The highly organized transverse (t)-tubule structures in ventricular myocardium might partially balance the abnormalities in the Ca^{2+} transients of G589D and ivs7-2A>G-CMs [34]. At the same time, it is also possible that the typical abnormality that we observed in G589D-cells, namely prolonged contraction time, could actually generate more severe symptoms due to a shortened relaxation time.

This is the first time that two different LQTS related mutations in the same gene are reported to result in differences in functional properties of the patient specific CMs. Additionally, this is the first report to demonstrate abnormal mechanical beating properties of LQTS-specific single CMs. Earlier, the mechanical abnormalities with increased diastolic phase have been reported at the level of a whole heart of LQTS patients [33] but the abnormal mechanical phenotype in LQTS specific single cells is a novel and rather unexpected finding. Here we demonstrate that the disease specific beating of the cells can be distinguished from the normal behavior of single CMs just by analyzing the mechanical features of the beating. This novel method for characterization of CMs may generate additional detailed information from the beating of the cells and also from LQTS in general. In addition, this simple detection method allows developing it further for high through-put screening for LQTS specific – and also other cardiac disease specific – CMs.

5. Conclusion

CMs derived from two symptomatic LQT1 patients carrying two different *KCNQ1* mutations presented different manifestations when their electrical or mechanical beating properties were analyzed. APDs were significantly prolonged in both types of LQT1-CMs, but spontaneous EADs were present only in G589D-CMs. Mechanical beating behavior of G589D-CMs presented mostly prolonged contraction phase while inv7-2A>G-CMs had a fairly normal contraction time, but failed to relax properly. These results also demonstrate that simply by analyzing the mechanical beating behavior of the cells, the diseased CMs can be distinguished from the normal ones, providing a simple platform for diagnostic applications using iPSC derived CMs in the future.

Supplementary data to this article can be found online at http://dx.doi.org/10.1016/j.ijcha.2015.04.008.

Conflicts of interest

None.

Acknowledgments

We thank Merja Lehtinen and Markus Haponen for technical support (University of Tampere, BioMediTech and School of Medicine, Tampere, Finland). Christine Mummery (Department of Anatomy and Embryology, Leiden University Medical Center, Leiden, The Netherlands) is acknowledged for providing END-2 cells.

Acknowledgement of grant support: The study was funded by the Finnish Funding Agency for Technology and Innovation (40345/11), Finnish Cardiovascular Foundation, Pirkanmaa Hospital District, Finnish Cultural Foundation Pirkanmaa Regional Fund and Tampere Graduate Program in Biomedicine and Biotechnology.

References

[1] Hedley PL, Jørgensen P, Schlamowitz S, Wangari R, Moolman-Smook J, Brink PA, et al. The genetic basis of long QT and short QT syndromes: a mutation update. Hum Mutat 2009;30(11):1486–511.
[2] Barhanin J, Lesage F, Guillemare E, Fink M, Lazdunski M, Romey G. KvLQT1 and IsK (minK) proteins associate to form the I_{Ks} cardiac potassium current. Nature 1996; 384(6604):78–80.
[3] Sanguinetti MC, Curran ME, Zou A, Shen J, Specter PS, Atkinson DL, et al. Coassembly of KvLQT1 and minK (IsK) proteins to form cardiac I_{Ks} potassium channel. Nature 1996;384(6604):80–3.
[4] Laksman ZWM, Hamilton RM, Chockalingam P, Ballantyne E, Stephenson EA, Gross GJ, et al. Mutation location effect on severity of phenotype during exercise testing in type 1 long-QT syndrome: impact of transmembrane and c-loop location. J Cardiovasc Electrophysiol 2013;24(9):1015–20.
[5] Splawski I, Shen J, Timothy KW, Lehmann MH, Priori S, Robinson JL, et al. Spectrum of mutations in long-QT syndrome genes: KVLQT1, HERG, SCN5A, KCNE1, and KCNE2. Circulation 2000;102(10):1178–85.
[6] Barsheshet A, Goldenberg I, O-Uchi J, Moss AJ, Jons C, Shimizu W, et al. Mutations in cytoplasmic loops of the KCNQ1 channel and the risk of life-threatening events: implications for mutation-specific response to Î²-blocker therapy in type 1 long-QT syndrome. Circulation 2012;125(16):1988–96.
[7] Fodstad H, Bendahhou S, Rougier J, Laitinen-Forsblom P, Barhanin J, Abriel H, et al. Molecular characterization of two founder mutations causing long QT syndrome and identification of compound heterozygous patients. Ann Med 2006;38(4): 294–304.
[8] Piippo K, Swan H, Pasternack M, Chapman H, Paavonen K, Viitasalo M, et al. A founder mutation of the potassium channel KCNQ1 in long QT syndrome: implications for estimation of disease prevalence and molecular diagnostics. J Am Coll Cardiol 2001;37(2):562–8.
[9] Aromolaran AS, Subramanyam P, Chang DD, Kobertz WR, Colecraft HM. LQT1 mutations in KCNQ1 C-terminus assembly domain suppress IKs using different mechanisms. Cardiovasc Res 2014;104:501–11.
[10] Takahashi K, Tanabe K, Ohnuki M, Narita M, Ichisaka T, Tomoda K, et al. Induction of pluripotent stem cells from adult human fibroblasts by defined factors. Cell 2007; 131(5):861–72.
[11] Yu J, Vodyanik MA, Smuga-Otto K, Antosiewicz-Bourget J, Frane JL, Tian S, et al. Induced pluripotent stem cell lines derived from human somatic cells. Science 2007; 318(5858):1917–20.
[12] Davis RP, Casini S, van den Berg CW, Hoekstra M, Remme CA, Dambrot C, et al. Cardiomyocytes derived from pluripotent stem cells recapitulate electrophysiological characteristics of an overlap syndrome of cardiac sodium channel disease. Circulation 2012;125(25):3079–91.
[13] Egashira T, Yuasa S, Suzuki T, Aizawa Y, Yamakawa H, Matsuhashi T, et al. Disease characterization using LQTS-specific induced pluripotent stem cells. Cardiovasc Res 2012;95(4):419–29.
[14] Itzhaki I, Maizels L, Huber I, Zwi-Dantsis L, Caspi O, Winterstern A, et al. Modelling the long QT syndrome with induced pluripotent stem cells. Nature 2011; 471(7337):225–9.
[15] Lahti AL, Kujala VJ, Chapman H, Koivisto A-P, Pekkanen-Mattila M, Kerkelä E, et al. Model for long QT syndrome type 2 using human iPS cells demonstrates arrhythmogenic characteristics in cell culture. Dis Model Mech 2012;5(2):220–30.
[16] Malan D, Friedrichs S, Fleischmann BK, Sasse P. Cardiomyocytes obtained from induced pluripotent stem cells with long-QT syndrome 3 recapitulate typical disease-specific features in vitro. Circ Res 2011;109(8):841–7.
[17] Matsa E, Rajamohan D, Dick E, Young L, Mellor I, Staniforth A, et al. Drug evaluation in cardiomyocytes derived from human induced pluripotent stem cells carrying a long QT syndrome type 2 mutation. Eur Heart J 2011;32(8):952–62.
[18] Moretti A, Bellin M, Welling A, Jung CB, Lam JT, Bott-Flügel L, et al. Patient-specific induced pluripotent stem-cell models for long-QT syndrome. NEJM 2010;363(15): 1397–409.
[19] Hoebe RA, Van Der Voort HTM, Stap J, Van Noorden CJF, Manders EMM. Quantitative determination of the reduction of phototoxicity and photobleaching by controlled light exposure microscopy. J Microsc 2008;231(1):9–20.
[20] Paredes RM, Etzler JC, Watts LT, Zheng W, Lechleiter JD. Chemical calcium indicators. Methods 2008;46(3):143–51.
[21] Fodstad H, Swan H, Laitinen P, Piippo K, Paavonen K, Viitasalo M, et al. Four potassium channel mutations account for 73% of the genetic spectrum underlying long-QT syndrome (LQTS) and provide evidence for a strong founder effect in Finland. Ann Med 2004;36(1):53–63.
[22] Ahola A, Kiviaho AL, Larsson K, Honkanen M, Aalto-Setälä K, Hyttinen J. Video image based analysis of single human induced pluripotent stem cell derived cardiomyocyte beating dynamics using digital image correlation. Biomed Eng Online 2014;7:13–39.
[23] Mummery C, Ward-van Oostwaard D, Doevendans P, Spijker R, van den Brink S, Hassink R, et al. Differentiation of human embryonic stem cells to cardiomyocytes: role of coculture with visceral endoderm-like cells. Circulation 2003;107(21): 2733–40.
[24] Wettwer E, Scholtysik G, Schaad A, Himmel H, Ravens U. Effects of the new class III antiarrhythmic drug E-4031 on myocardial contractility and electrophysiological parameters. J Cardiovasc Pharmacol 1991;17(3):480–7.
[25] Towart R, Linders JTM, Hermans AN, Rohrbacher J, van der Linde HJ, Ercken M, et al. Blockade of the I_{Ks} potassium channel: an overlooked cardiovascular liability in drug safety screening? J Pharmacol Toxicol Methods 2009;60(1):1–10.
[26] Rae J, Cooper K, Gates P, Watsky M. Low access resistance perforated patch recordings using amphotericin B. J Neurosci Methods 1991;37(1):15–26.
[27] Bombardini T, Gemignani V, Bianchini E, Venneri L, Petersen C, Pasanisi E, et al. Diastolic time–frequency relation in the stress echo lab: filling timing and flow at different heart rates. Cardiovasc Ultrasound 2008;6(15).
[28] Heijman J, Spätjens RL, Seyen SR, Lentink V, Kuijpers HJ, Boulet IR, et al. Dominant-negative control of cAMP-dependent I_{Ks} upregulation in human long-QT syndrome type 1. Circ Res 2012;110(2):211–9.
[29] Marx SO, Kurokawa J, Reiken S, Motoike H, D'Armiento J, Marks AR, et al. Requirement of a macromolecular signaling complex for beta adrenergic receptor modulation of the KCNQ1–KCNE1 potassium channel. Science 2002;295(5554):496–9.
[30] Doss M, Di Diego J, Goodrow R, Wu Y, Cordeiro J, Nesterenko V, et al. Maximum diastolic potential of human induced pluripotent stem cell-derived cardiomyocytes depends critically on I_{Kr}. PLoS One 2012;7(7):e40288.
[31] January CT, Moscucci A. Cellular mechanisms of early after depolarizations. Ann NY Acad Sci 1992;644(1):23–32.
[32] Spencer CI, Baba S, Nakamura K, Hua EA, Sears MAF, Fu C, et al. Calcium transients closely reflect prolonged action potentials in iPSC models of inherited cardiac arrhythmia. Stem Cell Rep 2014;3(2):269–81.
[33] Haugaa KH, Amlie JP, Berge KE, Leren TP, Smiseth OA, Edvardsen T. Transmural differences in myocardial contraction in long-QT syndrome: mechanical consequences of ion channel dysfunction. Circulation 2010;122(14):1355–63.
[34] Ferrantini C, Crocini C, Coppini R, Vanzi F, Tesi C, Cerbai E, et al. The transverse-axial tubular system of cardiomyocytes. Cell Mol Life Sci 2013;70(24):4695–710.